# Experimental Determination of Crack Driving Forces in Integrated Structures

Jun He*, Guanghai Xu*, and Z. Suo#

*Intel Corporation, 5200 NE Elam Young Parkway, Hillsboro, Oregon 97124

#Division of Engineering and Applied Sciences, Harvard University, Cambridge, MA 02138

**Abstract.** For a crack in a brittle material in an integrated structure, the driving force $G$ is the reduction of the elastic energy in the structure, associated with the crack extending per unit area. In principle, $G$ can be calculated by solving a boundary value problem. In practice, however, such a calculation is prohibitively difficult for integrated structures of complex architectures, diverse materials and small features. The calculated value of $G$ is suspect when deformation properties and residual stress fields are poorly characterized. On the other hand, it costs little to make many replicates of an integrated structure, so that massive full-structure testing is affordable. We describe an experimental method to determine $G$. A crack, assisted by molecules in the environment (e.g., moisture), often extends at a velocity $V$ increasing with the crack driving force $G$. The $V$-$G$ function is specific to a given material and its environment. Once determined, the same function applies when this material is integrated in a structure with other materials, provided environmental molecules reach the crack front. In the integrated structure, an observed crack velocity, together with the known $V$-$G$ function, provides a reading of the crack driving force. The observed crack velocity can be used to measure deformation properties of ultrathin films. We also describe a procedure to measure the crack driving force $G_R$ due to the residual stress field in the integrated structures, even when $G_R$ by itself is too low for the crack to extend at a measurable velocity.

## INTRODUCTION

A crack extends in a brittle material by breaking atomic bonds along the crack front. The physics of crack growth may well have been understood, from electrons to atoms and to microstructures. This statement by itself, however, is of limited value; it offers little help to the engineer trying to prevent cracking in an integrated structure. Hypes of multi-scale computation aside, no reliable method exists today to predict cracking by computation alone. The pragmatic approach is to divide the labor between computation and measurement within the framework of fracture mechanics [1]. Some quantities are easier to compute, and others easier to measure. A combination of computation and measurement solves problems economically.

Of course what is easy changes with circumstances. As new tools and applications emerge, it behooves us to negotiate a more economical division of labor. The history of the fracture mechanics makes an excellent case study of such divisions and their shifts. For the last few years, in the course of studying cracks in interconnect structures, we have found it necessary to make a new division of labor. This paper gives a preliminary account of our work.

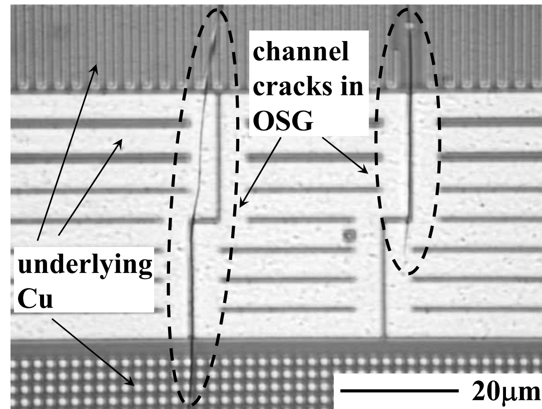


Figure 1. A plan view of a test structure shows two cracks running in an organosilicate glass (OSG) blanket film on top of a layer of Cu interconnects. A particularly weak OSG is used here to illustrate the impact of underlying metal pattern on OSG cracking.

Organosilicate glasses (OSGs), also known as carbon-doped oxides (CDOs), have recently been selected as low-permittivity dielectrics to replace silicon dioxide in on-chip interconnect structures [2, 3]. The OSGs are brittle. During fabrication and operation, an integrated structure acquires stresses from material deposition, thermal expansion, chemical-mechanical polishing, electromigration, etc. [4-7]. The stresses may cause the OSGs to grow cracks; Fig. 1 shows an example. Because the OSGs are selected for function and integration, because the mechanical behavior of OSGs is similar to many candidate materials for future device structures, and because few toughening strategies work at the small size scale [8], it is urgent to devise a protocol to prevent integrated structures from OSG cracking.

For a crack in a given structure, the crack driving force, $G$, is the reduction of the elastic energy in the structure associated with the crack extending per unit area, when the external mechanical load is rigidly held and does no work [1]. An existing protocol is to calculate $G$ by solving a boundary value problem. Such solutions are accumulating for thin film structures [9-16]. To prevent a crack from growing, the engineer must ensure that $G$ is below a threshold value. The latter is estimated from experimental measurements [1].

The calculation of $G$ is prohibitively difficult for three-dimensional structures that integrate diverse materials. This is particularly so when the stress-strain relations of the constitute materials, as well as the residual stress fields in the structures, are poorly characterized. On the other hand, compared to large structures such as airplanes and ships, small structures such as on-chip interconnects are inexpensive. It costs little to make many replicates of an integrated small structure, making massive full-structure testing practical. An integrated structure is an analog computer, and massive testing a form of parallel computing. Massive testing is a key to the success of the microelectronic industry to make reliable structures. These circumstances have motivated us to develop a method to measure the crack driving force experimentally.

Our method relies on a familiar phenomenon: moisture-assisted crack growth. Water (and some other molecules) in the environment may participate in the process

of breaking atomic bonds along the crack front [1]. For the environmental molecules to reach the crack front and to break atomic bonds there, the crack extends at a velocity much below the sound speed in the material. The crack velocity *V* is an increasing function of the crack driving force *G*. In recent years, such *V*-*G* functions have been measured for various dielectric films [17-25]. (Crack velocity as low as $10^{-12}\mathrm{m/s}$ has been measured [22]. Recall that sound speeds in solids are on the order of $10^{3}\mathrm{m/s}$. Also note that, to limit a crack to grow 100 nm in 10 years, the crack velocity must be below $3\times10^{-16}\mathrm{m/s}$.)

The *V*-*G* function is specific to a given material and its environment. Once determined, the same function applies when this material is integrated with other materials in a structure, provided the environmental molecules reach the crack front. In such an integrated structure, an observed crack velocity, together with the known *V*-*G* function, provides a reading of the crack driving force. The principle is analogous to that of a mercury thermometer. Mercury expands when temperature rises; the temperature-volume function can be calibrated. The volume of mercury provides a reading of the temperature.

## CALIBRATING THE *V-G* FUNCTION

Following Ma et al. [18], we measure the *V*-*G* function by observing the growth of a channel crack in an OSG film on a silicon substrate, subject to four-point bend (Fig. 2). A silicon substrate, about 750 $\mu$m thick, is polished to minimize crack-like flaws. The polished substrate can sustain stress well over 1 GPa. Deposit on the silicon substrate an OSG film, of thickness on the order of 1 $\mu$m. Measure the residual stress in the film, $\sigma_R$, by using the wafer curvature method [4]. Introduce initial flaws and then apply the stress in the film using a four-point fixture to bend the sample. Channel cracks emanate from the flaws. Measure the crack velocities using a digital camera. All tests reported in this work are conducted in an environmental chamber, at room temperature, with relative humidity of 30%. Figure 3 shows two representative micrographs.

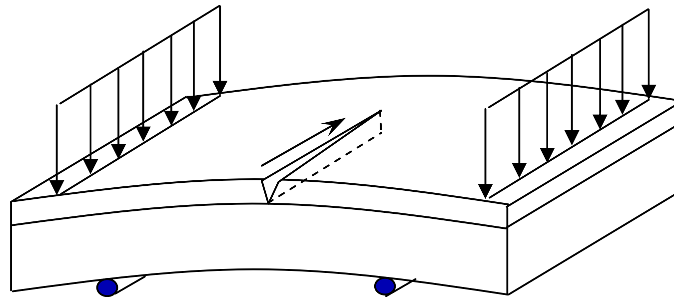

**FIGURE 2.** A schematic of the experimental setup. An OSG thin film is deposited on a silicon substrate. When the substrate is bent in a four-point bend fixture, a channel crack grows in the film. The front of the crack extends in the plane of the film, and the edge of the crack stops at the film/substrate interface. The film remains bonded to the substrate. Measure the crack velocity as a function of the bending load. The data calibrate the *V*-*G* function of the OSG.

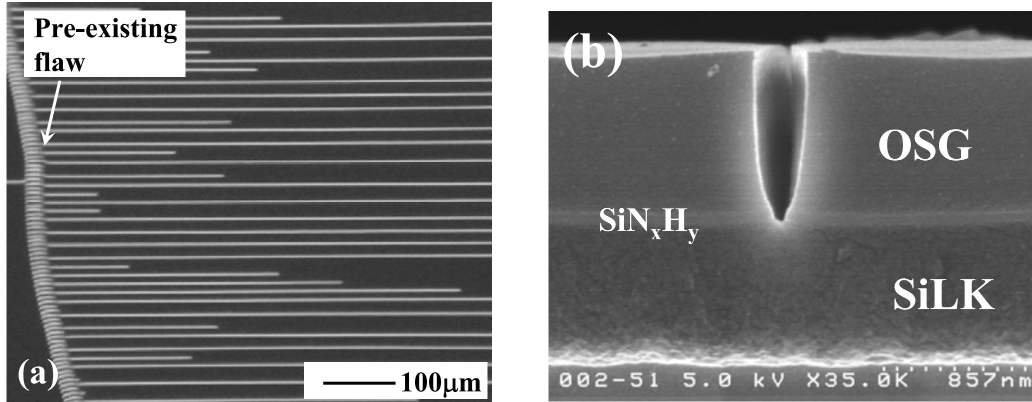


**FIGURE 3.** Channel cracks in two structures. (a) An array of channel cracks grow in a 2250 nm OSG film on a silicon substrate. The cracks initiate at different times from the flaws introduced by the scratch of a hard object. The crack velocity decreases with the crack spacing. (b) On a silicon substrate, a film stack comprises a 834 nm SiLK (a spin-on organic film), a 60 nm $SiN_xH_y$, and a 1061 nm OSG. A channel crack cuts across both the OSG and $SiN_xH_y$ films, arresting at the $SiN_xH_y$ /SiLK interface.

The level of the bending load is measured by the radius of curvature $R_B$ of the substrate caused by the load. This load is converted to the crack driving force as follows. The bending induces a tensile strain, $H/2R_B$, at the top surface of the substrate, where $H$ is the thickness of the silicon substrate. The film is bonded to the substrate: the bending also induces the same strain $H/2R_B$ in the film. The film is linearly elastic, with Young's modulus $E$ and Poisson's ratio $\nu$. Consequently, the bending induces an additional stress in the film:

$$\sigma_B = \bar{E}H/2R_B, \tag{1}$$

where $\bar{E} = E/(1-\nu^2)$ is the elastic modulus of the film in a state of plane strain deformation. The net stress in the film, $\sigma$, is the sum of the residual stress and the bending stressing: $\sigma = \sigma_R + \sigma_B$.

A dimensional consideration dictates that the crack driving force take the form

$$G = Z\sigma^2 h/\bar{E}, \tag{2}$$

where $h$ is the film thickness, and $Z$ is a dimensionless number. For an isolated channel crack in a thin film on a thick substrate, the number $Z$ varies with the elastic properties of the film and substrate, and has been calculated by solving the boundary value problem [11]. We take Young's modulus and Poisson's ratio for silicon to be 165 GPa and 0.28, and those for the OSG to be 8.33 GPa and 0.25. From [11], we find that $\boldsymbol{Z} = 1.096$.

Figure 4 gives the experimentally measured crack velocity $V$ as a function of the crack driving force $G$. Within the range of the measurement, our data fit an empirical relation:

$$V/V_* = \exp(G/G_*). \tag{3}$$

The fitting parameters are $V_* = 7.52 \times 10^{-16}$m/s and $G_*$ = 0.106 J/m$^2$. A small change in the crack driving force causes a large change in the crack velocity. Our experimental setup can readily measure crack velocity between $10^{-9}$ to $10^{-4}$m/s. The

*V-G* function is sensitive to the environment. The crack velocity depends on humidity for a crack in ambient, and on the concentration of hydroxyl ions and hydrogen peroxide for a crack in an aqueous solution [20-23]. Consequently, within the measurable velocity range, we can access a wide range of *G* by adjusting the environment. This preliminary account, however, does not pursue such an option.

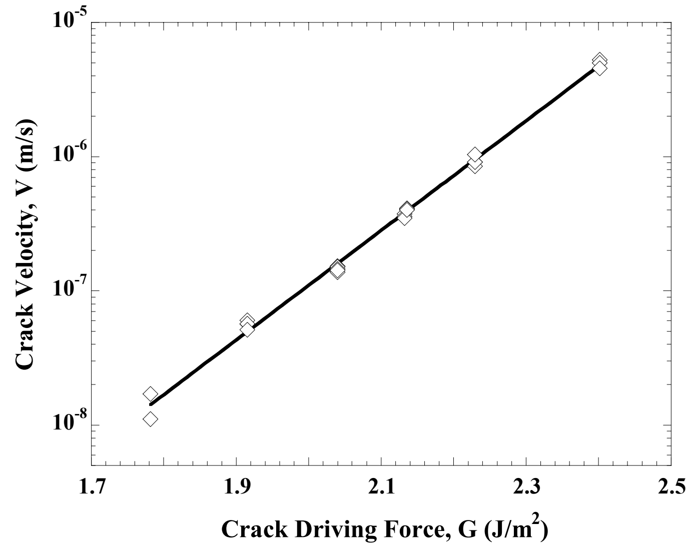


**FIGURE 4.** The *V-G* function measured by observing isolated channel cracks in an OSG film on a silicon substrate, subject to six levels of the bending load. Each data point corresponds to one of 27 crack velocity measurements.

## READING THE CRACK DRIVING FORCE

For a crack in the OSG in an integrated structure, an observed crack velocity, together with the *V-G* functions in Fig. 4, provides a reading of the crack driving force. The method is accurate because a small variation in *G* causes to a large variation in *V*. The method can readily measure the driving force *G* of a crack in a complex structure such as that in Fig. 1. To ascertain the accuracy of the measurement, we would need to calculate *G* by solving a boundary value problem, which is prohibitively difficult for a structure of this complexity. Instead, we use the multiple cracks in Fig. 3a as a demonstration of the method. In this case, the complexity arises from the multiple cracks, for which the mechanics is established. The measured velocity of isolated cracks as a function of the bending load calibrates *V-G* function, as given in Fig. 4. At a fixed bending load, cracks initiate at different times. A new crack grows in a film stripe between two old cracks, whose fronts are much farther ahead. Because the old cracks partially relieve the stress in the stripe, the driving force for the new crack is lower than that for the old cracks. Consequently, the crack velocity decreases with the crack spacing. When the velocity of a new crack is measured, the *V-G* function in Fig. 4 provides a reading of *G* for this crack.

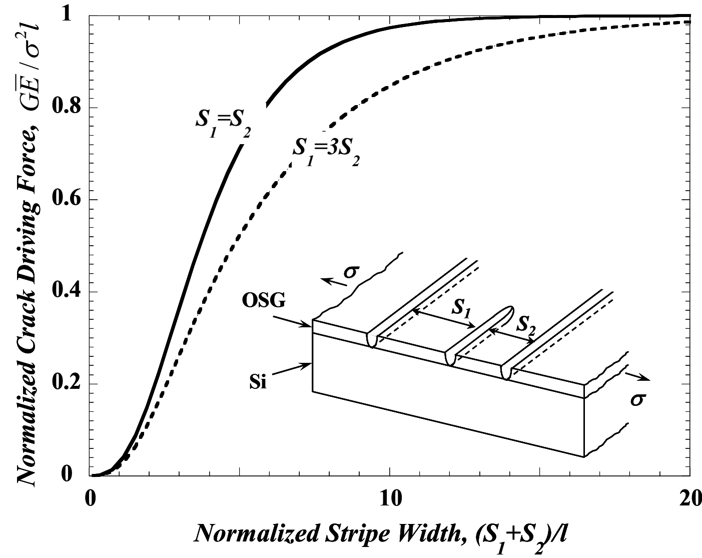


**FIGUER 5.** The normalized crack driving force as a function of the normalized stripe width, as calculated from a shear lag model.

To ascertain the accuracy of $G$ so measured, following Xia and Hutchisnon [13], we calculate $G$ for a crack extending between two old cracks. Consider the film stripe, of width $S$, between the two cracks. Near either crack, the stress in the stripe is partially relived. According to a shear lag model, the elastic energy stored per unit length of the stripe and the substrate underneath is

$$U(S) = wSh - \frac{\sigma^2 lh}{\bar{E}} \tanh\left(\frac{S}{2l}\right), \tag{4}$$

where $w$ is the elastic energy density, and $\sigma$ the net film stress, in the uncracked blanket film. The length $l$ scales with the width of the zone in which the stress is significantly relieved.

Next consider a new crack growing in the stripe, at distances $S_1$ and $S_2$ from the two old cracks (Fig. 5). Far ahead the new crack front, the elastic energy per unit length is $U(S_1 + S_2)$. Far behind, the new crack splits the stripe into two, and the elastic energy per unit length is $U(S_1) + U(S_2)$. By definition, the driving force for the new crack, $G$, is the reduction of elastic energy in the structure associated with the new crack extends per unit area: $Gh = U(S_1 + S_2) - U(S_1) - U(S_2)$. This gives

$$G = \frac{\sigma^2 l}{\bar{E}}\left[\tanh\left(\frac{S_1}{2l}\right) + \tanh\left(\frac{S_2}{2l}\right) - \tanh\left(\frac{S_1 + S_2}{2l}\right)\right]. \tag{5}$$

Figure 5 plots the crack driving force as a function of the stripe width. The crack driving force increases with the stripe width, and approaches a plateau when the stripe width exceeds some multiple of the relaxation length. A crack along the centerline of the stripe has a higher driving force than that running near either edge of the stripe. For Eq. (5) to recover the driving force for an isolated crack, Eq. (2), following Xia and Hutchinson [13], we will set the relaxation length to be $l = Zh$.

**Table 1. Experimental values of film stress, crack spacing, and crack velocity plotted in Fig.6**

| Crack | A | B | C | D | E | F | G | H | I | J | K | L | M | N | O | P |
|---|---|---|---|---|---|---|---|---|---|---|---|---|---|---|---|---|
| $\sigma$ (MPa) | 96.6 | 93.0 | 96.7 | 96.7 | 96.7 | 93.0 | 96.5 | 96.5 | 93.0 | 93.0 | 96.5 | 93.0 | 93.0 | 93.0 | 93.0 | 93.0 |
| $S_1$ (μm) | 7.8 | 6.0 | 7.5 | 7.5 | 7.7 | 8 | 7 | 7..5 | 8.5 | 10.5 | 8.0 | 11 | 20 | 16 | 20 | 20 |
| $S_2$ (μm) | 5.0 | 8.0 | 5.8 | 6.0 | 5.7 | 7.8 | 6.7 | 7.5 | 8.8 | 10.5 | 8.0 | 11.5 | 11.3 | 17 | 18 | 20 |
| $V$ (μm/s) | 0.010 | 0.013 | 0.035 | 0.036 | 0.043 | 0.061 | 0.084 | 0.196 | 0.256 | 0.625 | 0.943 | 1.67 | 2.86 | 3.85 | 3.85 | 4.17 |

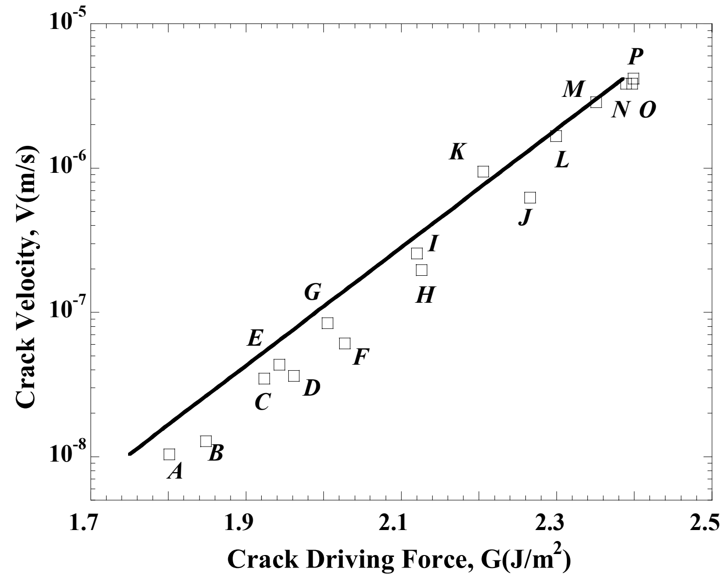


FIGUER 6. The solid line is the *V-G* function established by isolated cracks in the OSG film. Each data point corresponds to one of the 16 cracks in a film stripe, plotting the observed crack velocity against the crack driving force calculated from Eq. (5), using the observed crack spacings, as well as the stress, thickness and modulus of the OSG film.

In the experiment, we follow 16 cracks in various film stripes, recording the spacings $S_1$ and $S_2$, as well as the net film stress (Table 1). Such data are used to calculate the crack driving forces from Eq. (5). Figure 6 plots the crack driving force calculated this way against the observed crack velocity. The agreement with the *V-G* function determined from the isolated cracks is excellent.

## MEASURING ELASTIC MODULUS

In an integrated structure, the driving force for a crack in one material may depend on deformation properties of all constituent materials. Consequently, the measured crack velocity can provide a reading of deformation properties. For example, we can measure Young's modulus of a thin film by using two test configurations. First, measure the *V-G* function of a thin film by using a test configuration in which *G* is

*independent* of the elastic constants of the film. This independence is a common feature for any specimen consisting of a thin film sandwiched between two thick substrates [21-24]. Then, separately measure the crack velocity for the same film in the channel crack configuration, Fig. 2. Using the known *V-G* function, the measured channel crack velocity provides a reading for $G$. For a channel crack, $G$ does depend on Young's modulus of the film, Eq. (2). Young's modulus can thus be deduced.

The above method assumes that the *V-G* functions in the two test configurations (i.e., the sandwich and the channel crack) are identical. This assumption can be wrong if the film is anisotropic. (The crack in the film is parallel to the substrate surface in the sandwich configuration, but perpendicular to the substrate surface in the channel crack configuration.) Care should also be taken to minimize the effect of plasticity of adjacent layers, and to ensure that, in the sandwich configuration, the crack runs inside the desired material, rather than on one of the interfaces.

We find it possible to estimate Young's modulus of the film by just using the channel crack velocity measurements alone. The relaxation length $l$ increases with the ratio of the elastic modulus of the film to that of the substrate. Consequently, the velocities of multiple channel cracks contain the information of Young's modulus of the film. Figure 7 plots the same data in Figs. 4 and 6 again, using three assumed values of Young's modulus for the OSG. According to the elasticity solution [11], for the three assumed values of Young's modulus of the OSG film, 5.4 GPa, 7.4 GPa and 9.0 GPa, the corresponding $Z$-vales are 1.078, 1.090 and 1.100. The *V-G* function is material-environment specific. Consequently, the data points for the 16 cracks in finite stripes should collapse onto the solid line established by the isolated cracks. By this criterion, $E$ = 7.50 GPa is a better choice than either $E$ = 9.0 GPa or $E$ = 5.4 GPa.

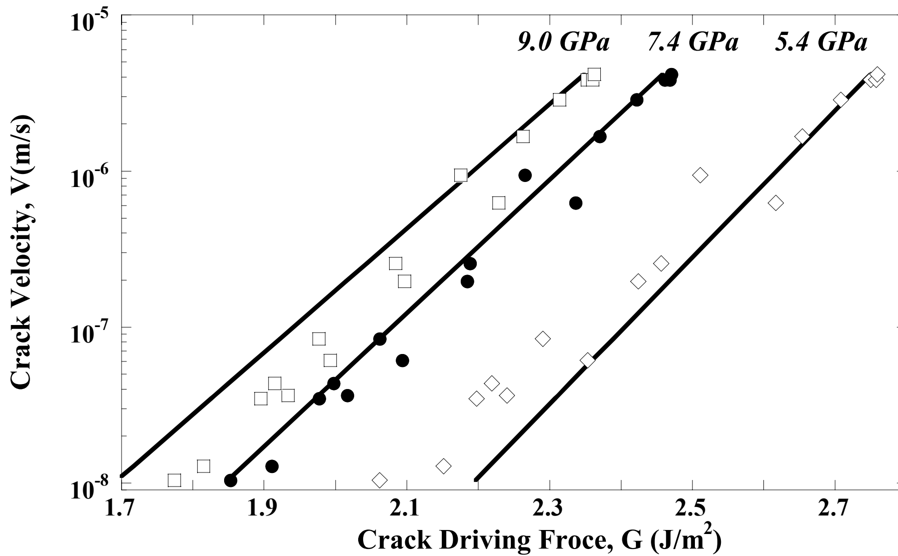


**FIGUER 7.** The same data sets as in Figs. 4 and 6, plotted using three assumed values of OSG Young's modulus. Each solid line is the *V-G* function established by isolated cracks. Each data point corresponds to one of the 16 cracks in a film stripe, plotting the observed crack velocity against the crack driving force calculated from Eq. (5), using the observed crack spacings, as well as the stress, thickness and modulus of the OSG film.

Two cautionary notes should be made. First, Eq. (5) is derived from the shear lag model, whose accuracy has not been evaluated for a complaint film on a stiff substrate. Second, when the film is less stiff than the substrate, as for OSG on silicon, the value of Z varies slowly with the film-to-substrate modulus ratio. Consequently, we do not expect this method to provide an accurate measurement of Young's modulus in this case. By contrast, when the modulus of the film exceeds about 10% that of the substrate, $Z$ varies more significantly with the film-to-substrate modulus ratio, so that the observed velocities of multiple channel cracks will provide an accurate measurement of Young's modulus of the film.

## MEASURING YIELD STRENGTH

The observed crack velocity can also provide a reading for the yield strength. To illustrate the idea, consider the film stack shown in Fig. 3b, consisting of OSG, $SiN_xH_y$ and SiLK films on a silicon wafer. The SiLK is a plastically deformable organic [26], with Young's modulus 3.1 GPa and yield strength about 50 MPa measured by nano-indentation. Fig. 8 plots the measured crack velocity as a function of a loading parameter. The data are impressive when compared with those for the OSG film by itself on silicon substrate. Evidently, the introduction of the SiLK underlayer makes the OSG film more vulnerable to cracking.

The remarkable difference is caused by the low modulus and the low yield strength of the SiLK underlayer. Fig. 9 plots the normalized crack driving force, $G\overline{E}/h\sigma^2$, determined from the crack velocities, as a function of the stress in the OSG film. Also plotted is the value of $G\overline{E}/h\sigma^2$ calculated using the finite element method, assuming that SiLK is linearly elastic. This value $G\overline{E}/h\sigma^2$ = 1.53, as compared to $Z$ = 1.096 for the OSG on silicon, shows the effect of an underlayer of a low elastic modulus on the crack driving force. As evident in Fig. 9, the elastic effect, however, does not account for the measured crack driving force. We attribute the difference to plastic deformation in the SiLK underlayer.

For a channel crack in an elastic film on an elastic and perfectly plastic underlayer, the driving force is given by [9]

$$\frac{G\overline{E}}{\sigma^2 h} = A + \frac{\sigma}{\sqrt{3}\sigma_Y}, \tag{6}$$

where the constant $A$ accounts for the elastic deformation, and $\sigma_Y$ is the yield strength of the SiLK underlayer. From the slope of the data line in Fig. 9, we estimate that $\sigma_Y = 23\text{MPa}$. From the magnitude of the data line, we estimate that $\sigma_Y = 41.6 \text{ to } 46.7\text{MPa}$. Both estimates are somewhat lower than that reported in the literature as well as values obtained by nano-indentation. The discrepancy might be due to the residual stress in the SiLK underlayer, and to Eq. (6) used to analyze the data. The latter was derived from an approximate model. Also, we have neglected the $SiN_xH_y$ layer in our analysis. A comprehensive analysis of these effects will be reported elsewhere.

These cautionary remarks aside, Fig. 8 reflects a large difference in the observed crack velocity in OSG on silicon substrate and that in OSG on SiLK underlayer. Once

the mechanics solution is cleaned up, the channel crack velocities will provide sensitive readings of mechanical properties of ultrathin films. This new method will complement, or even surpass, the existing methods, such as nanoindentation, wafer curvature and acoustic methods. An evaluation of this exciting prospect is in progress.

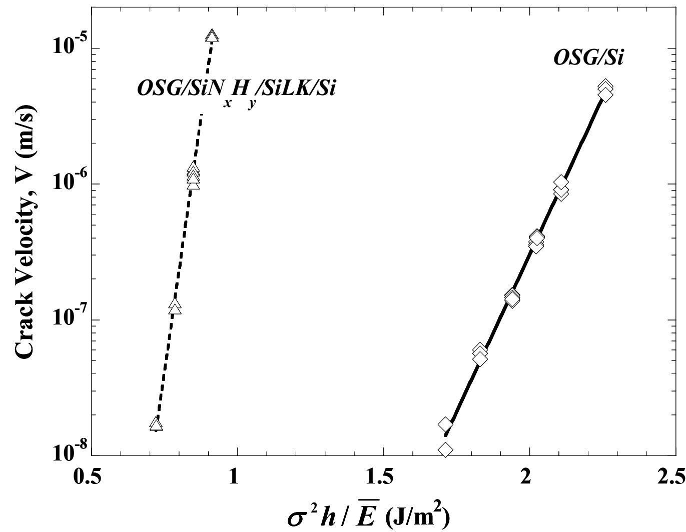


**FIGURE 8.** The measured crack velocity as a function of a loading parameter. Two cases are compared: OSG/Si and OSG/SiN/SiLK/Si. The latter is more vulnerable to cracking.

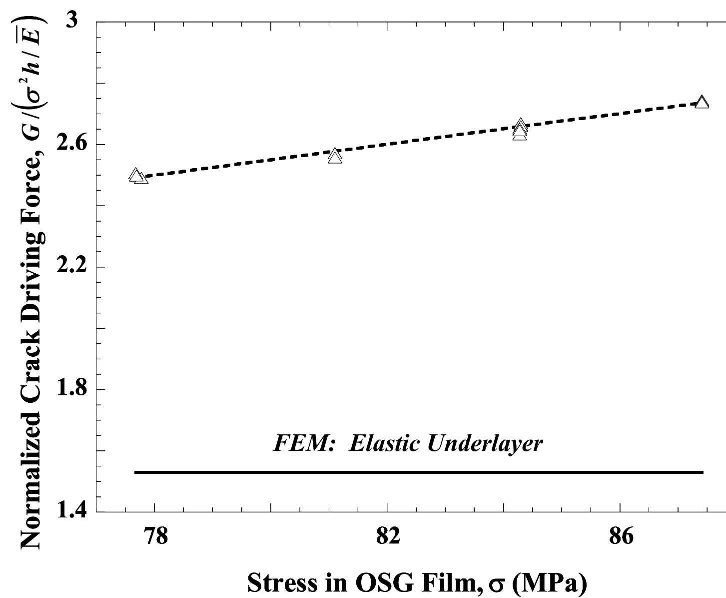


**FIGURE 9.** The normalized crack driving force for an OSG film on a SiLK layer as a function of the stress in the OSG film. The data points are the readings from the observed crack velocity. The solid line in the lower part of the figure is calculated from the finite element method, assuming the SiLK underlayer is linearly elastic.

## CRACK DRIVING FORCE DUE TO RESIDUAL STRESS FIELD

A crack may grow slowly in a structure under the residual stress field, so that the structure remains functional for a long time, and then fails suddenly. Several factors make the risk assessment difficult. First, the residual stress field is generated by material deposition, thermal expansion, electromigration, etc. An accurate determination of the residual stress field is usually impossible for complex structures. Second, calculations based on continuum mechanics are tedious, and the results are unreliable because material properties are usually not well characterized. Third, if the crack driving force due to the residual stress field is low, the crack velocity may be too low to be observed within a reasonable testing time.

To circumvent these difficulties, we can proceed as follows. An equivalent measure of the crack driving force is the stress intensity factor, *K*, which relates to *G* as $G = K^2 / \bar{E}$. The known *V-G* function can be converted to the *V-K* function. Denote the stress intensity factor associated with the residual stress field by $K_R$, which is too low for the crack to grow at a measurable velocity. Subject the sample to a bending load *F* to generate measurable crack velocity, which provides a reading of the stress intensity factor, *K*. Provided the bending does not induce significant nonlinear deformation in the thin film structure, the stress intensity factor is a linear function of the bending load *F*, namely,

$$K = K_R + BF, \tag{7}$$

where *B* is the slope. Several measurements of *K* at different levels of bending load *F* are sufficient to establish this straight line on the coordinate plane (*K, F*). The intercept of the straight line on the *K*-axis is the stress intensity factor $K_R$ due to the residual stress. To ensure that the crack will not grow under the residual stress, we must ensure that $K_R$ is below a threshold value. The latter may be estimated from the experimental record of the *V-G* function at exceedingly small velocities.

## CONCLUDING REMARKS

This work is motivated by two considerations concerning integrated small structures: (1) the crack driving force *G* is prohibitively difficult to calculate, and (2) massive full-structure testing is affordable. We describe a method to determine *G* experimentally by measuring crack velocities. The method can measure *G* in complex structures, subject to residual stress fields. The method can also measure deformation properties of ultrathin films. Because the observed crack velocity provides a sensitive reading of the crack driving force, we suspect that, in the examples given, the uncertainties in the property readings result more from inaccuracy of the models than from experimental errors. Once the mechanics solutions are cleaned up, the channel crack velocities will provide sensitive readings of mechanical properties of ultrathin films. This new method will complement, or even surpass, the existing methods, such as nanoindentation, wafer curvature and acoustic methods.

Several immediate implications of this method should not escape our readers. First, since the crack velocity plays a central role, high-resolution and automatic techniques

to measure crack velocity becomes valuable. Exiting techniques have been reviewed recently [22]; they need be adapted to channel cracks. Second, values will depreciate somewhat for brute force efforts to compute $G$ for complex integrated structures, so long as they remain more costly and less credible than measurements. Third, to use the crack velocities to determine deformation properties, property-sensitive test configurations need be developed.

## ACKNOWLEDGMENTS

ZS acknowledges the financial support of the NSF MRSEC and the Division of Engineering and Applied Sciences at Harvard University.

## REFERENCES

1. B. Lawn, *Fracture of Brittle Solids*. Cambridge University Press (1993).
2. K. Maex, M.R. Bakanov, D. Shamiryan, F. Iacopi, S.H. Brongersma and Z.S. Yanovitskaya, *J. Appl. Phys*. **93**, 8793-8841 (2003).
3. M.A. Hussein and Jun He, *IEEE Trans. Semicond. Manufact*. In press (2004).
4. W.D. Nix. *Metall. Trans.* **20A**, 2217-2245 (1989).
5. Z. Suo, pp. 265-324 in Volume 8: *Interfacial and Nanoscale Failure* (W. Gerberich, W. Yang, Editors), *Comprehensive Structural Integrity* (I. Milne, R.O. Ritchie, B. Karihaloo, Editors-in-Chief), Elsevier, Amsterdam, 2003.
6. L.B. Freund and S. Suresh. *Thin Film Materials: Stress, Defect Formation and Surface Evolution.* Cambridge University Press, UK (2003).
7. J.J. Vlassak. *J. Mech. Phys. Solids* **52,** 847-873 (2004).
8. D.A. Maidenberg, W. Volksen, R.D. Miller and R.H. Dauskardt. In press.
9. M.S. Hu and A.G., Evans, *Acta Metall.* **37**, 917-925 (1989).
10. J.W. Hutchinson and Z. Suo, *Advances in Applied Mechanics* **29**, 63-161 (1991).
11. J.L. Beuth, *Int. J. Solids Structures* **29**, 1657-1675 (1992).
12. J.L. Beuth and N.W. Klingbeil, *J. Mech. Phys. Solids* **44**, 1411-1428 (1996).
13. Z.C. Xia and J.W. Hutchinson, *J. Mech. Phys. Solids* **48**, 1107-1131 (2000).
14. J.M. Ambrico, E.E. Jones and M.R. Begley, Int. J. Solids Structures **39**, 1443-1462 (2002).
15. R. Huang, J.H. Prévost, Z.Y. Huang and Z. Suo, *Engineering Fracture Mechanics* **70**, 2513-2526 (2003).
16. J.J. Vlassak, *Int. J. Fracture* **119/120**, 299-323 (2003).
17. Q. Ma, *J. Mater. Res*. **12**, 840-845 (1997).
18. Q. Ma, J. Xie, S. Chao, S. El-Mansy, R. McFadden and H. Fujimoto, *Mater. Res. Soc. Symp. Proc*. **516**, 331-336 (1998).
19. Guanghai Xu; Jun He, E. Andideh; J. Bielefeld and T. Scherban, *Proc of the 2002 International Interconnect Technology Conference*, pp 57-59, June 7-9, San Francisco, California (2002).
20. R.F. Cook and E.G. Liniger, *J. Electochem. Soc*. **146**, 4439-4448 (1999).
21. E. P. Guyer and R. H. Dauskardt, *Nature Materials* **3**, 53-57 (2004).
22. E. P. Guyer and R. H. Dauskardt, submitted for publication.
23. J.J. Vlassak, Y. Lin and T.Y. Tsui, submitted for publication.
24. M.W. Lane, X.H. Liu and T.M. Shaw, *IEEE Transactions on Device and Materials Reliability* **4**, (2004). In press.
25. X.H. Liu, T.M. Shaw, M.W. Lane, R.R. Rosehnberg, S.L. Lane, J.P. Doyle, D. Restaino, S.F. Vogt and D.C. Edelstein, *Proc of the 2004 International Interconnect Technology Conference*, pp 93-95, June 7-9, San Francisco, California (2004).
26. S.J. Martin, J.P. Godschalx, M.E. Mills, E.O. Shaffer and P.H., Townsend. *Advanced Materials* **12**, 1769-1778 (2000).